

# Exploring the relationship between SDNR and detectability in dual-energy breast x-ray imaging

Roshan Karunamuni<sup>1</sup>, Swathiu Kanamaluru<sup>2</sup>, Kristen Lau<sup>1</sup>, Sara Gavenonis<sup>1</sup>, Predrag R. Bakic<sup>1</sup>,  
Andrew D.A. Maidment<sup>1</sup>

1. Department of Radiology, University of Pennsylvania, Philadelphia, PA 19104
2. School of Biomedical Engineering, Science, Drexel University, Philadelphia, PA 19104  
aros@seas.upenn.edu

## ABSTRACT

Contrast-enhanced (CE) digital breast tomosynthesis (DBT) provides a technique to increase the contrast of radiographic imaging agents by suppressing soft-tissue signal variation. By reducing the effect of the soft-tissue anatomical noise, it is then possible to quantify the signal from an iodinated contrast agent. The combination of dual-energy and tomographic acquisitions allows for both the accurate quantification and localization of an iodinated lesion. Here, we present our findings demonstrating the relationship that exists between the signal difference to noise ratio (SDNR) and reader detectability of iodinated lesions in a physical anthropomorphic phantom. The observer study was conducted using the ViewDEX software platform with a total of nine readers. The readers were asked to score each of the iodinated lesions on a scale from 1 (entire boundary and area are visible) to 5 (not visible). Both SDNR and lesion detectability were found to improve as the concentration of the iodine increases, and the thickness of the phantom decreases. Lesion detectability was better in the tomographic slice that best matches the focal plane of the imaged object. However, SDNR does not significantly change with focal plane. Our results demonstrated that observer lesion detectability correlated well with SDNR. Lesions whose SDNR fell below 1 were difficult to distinguish from the background and were in general not visible. Lesions that were rated entirely visible corresponded to those with SDNR values above 3. Lesions with intermediate SDNR values were visualized but not confidently from the surrounding background. These threshold SDNR values can be used to optimize the imaging parameters in CE-DBT.

**Keywords:** dual energy, x-ray tomosynthesis, SDNR, detectability, physical phantoms

## 1. INTRODUCTION

Contrast imaging has been used to explore angiogenesis in breast carcinoma by tracking the uptake and washout of contrast agents in tissues. Currently, magnetic resonance imaging (MRI), coupled with gadolinium chelated agents, is the preferred imaging technique to provide the vascular information that can later be used in the assessment and staging of breast cancer [1-3]. However, contrast-enhanced breast MRI is expensive and time-consuming while possessing a lower spatial resolution to breast x-ray imaging procedures such as mammography and digital breast tomosynthesis (DBT). Contrast-enhanced DBT (CE-DBT) is an emerging imaging modality designed to provide quantitative contrast information in a high-resolution 3-dimensional view of the breast [4-5]. The unique combination of functional information and high spatial resolution anatomical information in a single imaging procedure represents a powerful breast imaging tool. Clinically, CE-DBT has been shown to provide morphological and vascular characterization of breast lesions that is concordant with DM and MRI [6-7].

The essence of CE-DBT is to acquire low- and high- energy images of the breast, and combine the images in order to remove the background soft-tissue signal variation so as to enhance conspicuity of the iodinated tumor. The two energy windows are placed on either side of the k-edge of iodine (33.2 keV) to make use of the sudden increase in attenuation coefficient compared to soft tissue. The low- and high- energy images are then subtracted using a weighting factor to yield a dual-energy (DE) image in which the background signal has been suppressed to facilitate quantification and segmentation of iodine-enhanced lesions.

The ability of CE-DBT to enhance tumors effectively is strongly dependent on the careful selection of imaging parameters such as peak voltage, filter choice, weighting factors, and dose-distributions. Thus, there has been a

significant effort to optimize the image acquisition of CE-DBT [8-10]. The majority of these studies use signal difference to noise ratio (SDNR) as a figure of metric to compare various combinations of imaging parameters. However, SDNR quantifies the detectability of an object by an ideal observer, in which the signal of the object is compared to that of the background normalized by the variance of those signals. The purpose of this work is to correlate SDNR in CE-DBT with a metric of real observer detectability that is more directly related to diagnostic performance.

## 2. METHOD

### 2.1 Physical Phantom Imaging

A previously developed anthropomorphic breast phantom [11] was used in this study. The phantom consists of removable sections that can be stacked together to simulate a breast of 5 cm compressed thickness with a 45% average volumetric density.

The phantom allows for flexibility in three separate parameters:

- **Thickness:** The total thickness can be varied by removing sections or adding sheets of plain acrylic. The total thickness of the phantom was varied from 10 to 95 mm
- **Iodine Concentration:** One section of the phantom was reproduced with ten embedded iodinated lesions whose areal concentrations,  $C$ , ranged from 1.03 to 4.83 mg/cm<sup>2</sup>. Two volumetric concentrations of iodine (5.03 and 2.57 mg/cm<sup>3</sup>) were used to create the lesions with various values of  $C$ . A map of the iodinated lesions as well as an example reconstructed tomographic slice of the phantom is shown in Figure 1.
- **Focal Plane:** The lesions are divided into two groups (G1 and G2) located on opposite sides of the iodinated section. These allocation of lesions between the two groups is demonstrated in Figure 1.

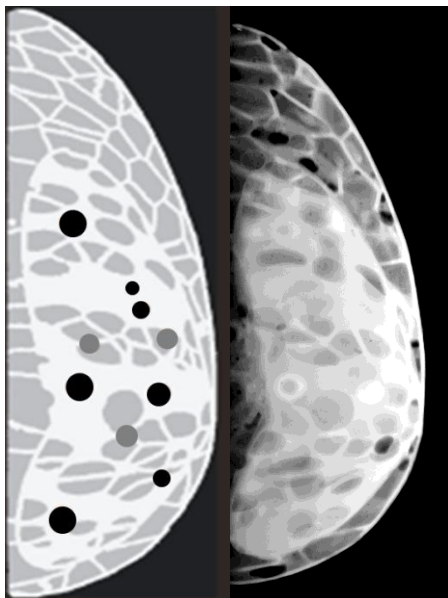


**Figure 1. Left** - Distribution of iodine spots between the two groups (G1 - gray and G2 - black) within the iodine inset. **Right** – A reconstructed slice of a low-energy tomographic acquisition of the phantom section with iodinated lesions.

**Imaging:** The phantom was imaged using a prototype Hologic Dimensions contrast-enhanced CE-DBT acquisition system. Eleven low- and high- energy pairs are acquired alternately, in a single sweep of 7.3 seconds. The applied voltage is set at 32 and 49 kVp for the low- and high-energy images, respectively. A copper filter is used for the high-energy image, whereas a rhodium filter is used for the low-energy acquisition. The mAs is automatically increased with increasing breast thickness to ensure an acceptable dose to the breast and adequate signal to the detector. Pre- and post-contrast image sets were acquired by carefully removing or adding the iodinated section without altering the position of the phantom on the detector to prevent registration artifacts.

**Processing:** A flowchart of the overall imaging and processing method used in the study is shown in Figure 2. A filtered back-projection algorithm was used to reconstruct tomographic slices from the flat-fielded projection data. A weighted subtraction is performed on the reconstructed low- and high- energy images to create a DE image set. The pre- and post-DE images were then subtracted to create a hybrid DE (HDE) image. This was done to remove the effects of scatter and other artifacts that were otherwise present in the DE image.

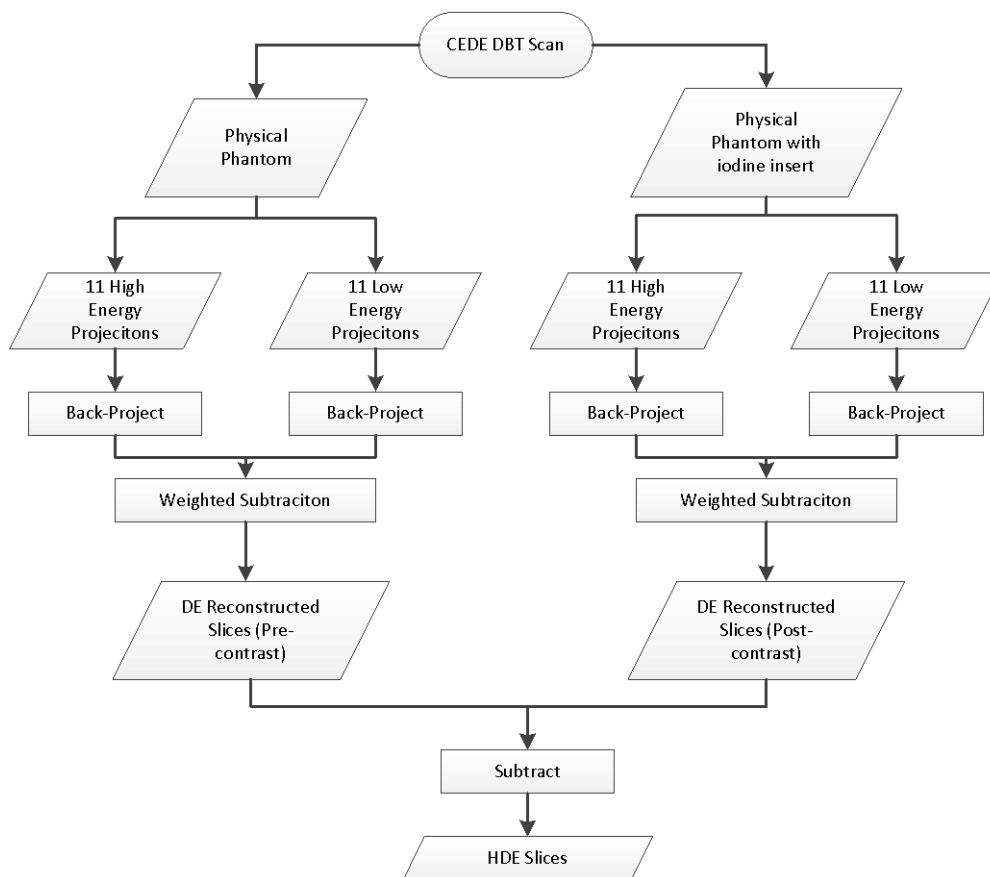


**Figure 2** A pre- and post-contrast image set, consisting of a low- and high-energy image, are taken by removing or inserting the iodine section of the physical phantom. The DE subtractions from the two time points (pre- and post-) are then subtracted to yield a HDE tomographic set.

For each phantom thickness, two representative slices (F1 and F2) from the tomographic reconstruction were used for both the SDNR and observer study measurements. These two slices, F1 and F2, roughly correspond to the two lesion groups G1 and G2, respectively.

**Analysis:** For all combinations of iodine concentration and total phantom thickness, the per-pixel SDNR was calculated as:

$$SDNR = \frac{SI_i - SI_b}{\sqrt{\sigma_b^2 + \sigma_i^2}} \quad (1)$$

Where SI represents the signal intensity and  $\sigma$  is the standard deviation of either the iodine lesion ( $i$ ) or background tissue ( $b$ ). In the amorphous selenium detector used by Hologic, the correlation between pixels can be assumed to be 0. Thus, the per-pixel SDNR is a complete descriptor of the signal and noise in the image.

## 2.2 Observer Study

The software tool ViewDEX [12] was used to rate observer detectability for each of the iodinated lesions. The task panel included the checkboxes for the readers to score each of the lesions, as well as the grading scheme (seen in Table 1) and

display options (Window/Level, Pan). The display section accommodated 3 different sizes of image display. A screenshot of the final ViewDEX interface is shown in Figure 3.

A total of 9 readers participated in this study. Each reader scored each iodine spot using the grading scheme outlined in Table 1. The readers were made aware of the locations of the iodine lesions through a printed map of the lesions. Each reader first participated in a training session in which HDE images similar to those used in the study were presented. This was done so as to reach consensus on what the various grading scores represented.

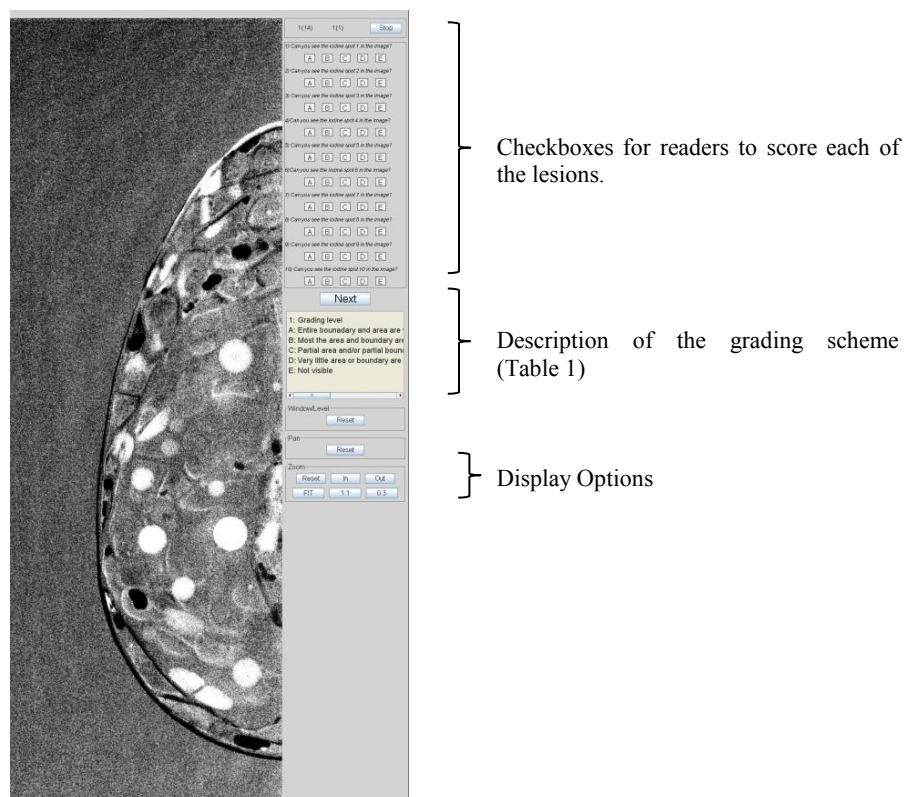


**Figure 3.** Screenshot of the ViewDEX interface used in the observer study. The image is shown on the left, and the user is asked to provide a score for each lesion using the checkboxes on the right.

**Table 1.** Grading scheme for iodine lesions in physical phantom.

Score	Description
1	Entire boundary and area are visible
2	Most of the area and boundary are visible and certain of the size of the lesion
3	Partial area and boundary are visible but unsure of the size of the lesion
4	Very little area or boundary are visible
5	Not visible

### 3. RESULTS

#### 3.1 Effect of concentration and thickness

SDNR was calculated for all breast thicknesses from 10 to 95 mm. The results for 10 and 70 mm thicknesses are shown in Figure 4. SNDR was found to increase with increasing areal concentrations of iodine for all thicknesses. The slope,  $S$ , of the linear fit that describes the relationship between SDNR and iodine concentration is plotted in Figure 5 for all phantom thicknesses.  $S$  is shown to decrease linearly with increasing phantom thickness.

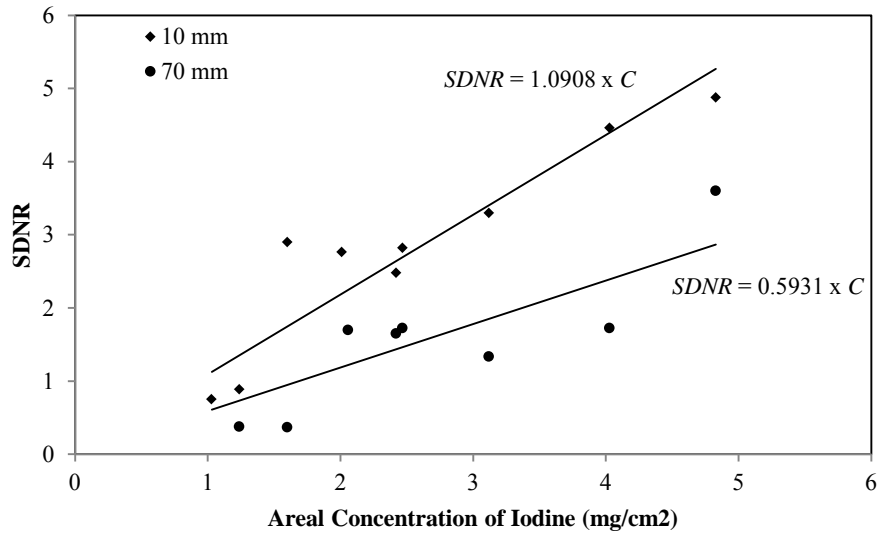


**Figure 4.** SDNR of lesions plotted against the areal concentration of iodine for 10 and 70 mm total thicknesses. The SDNR was found to increase linearly with the concentration of iodine regardless of the thickness of the phantom.

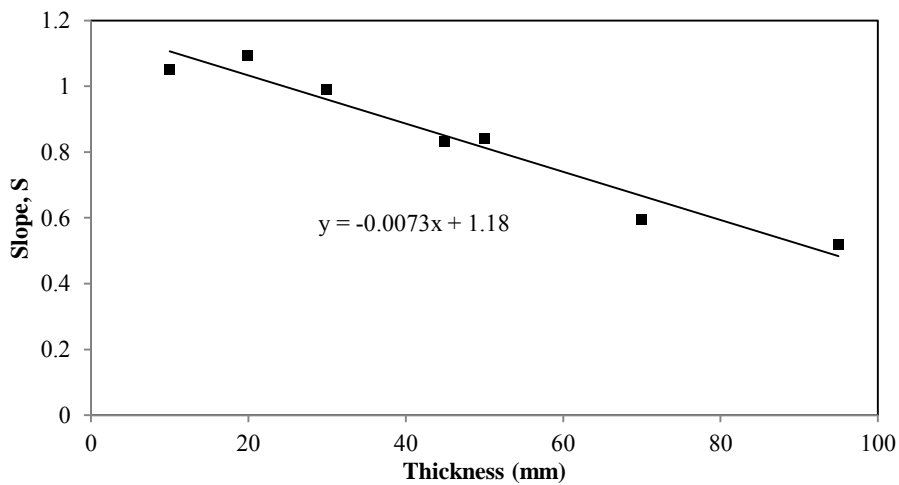


**Figure 5.** The sensitivity,  $S$ , plotted as a function of phantom thickness.  $S$  is calculated as the slope of the linear relationship between SDNR and areal concentration of iodine. As the thickness of the phantom increases,  $S$  decreases.

The visibility score was averaged over all the readers and plotted in Figure 6 for two concentrations of iodine lesions (4.83 and 1.03 mg/cm<sup>2</sup>) over the complete range of phantom thicknesses. At all thicknesses, the average reader score decreases as the areal concentration of lesion increases indicating that the lesions become more visible. In addition, at all concentrations of iodine lesions, the average reader score increases as the total phantom thickness increases indicating that the lesions are more difficult to detect in thicker breasts. However, this dependence is more prominent at the lower concentrations.

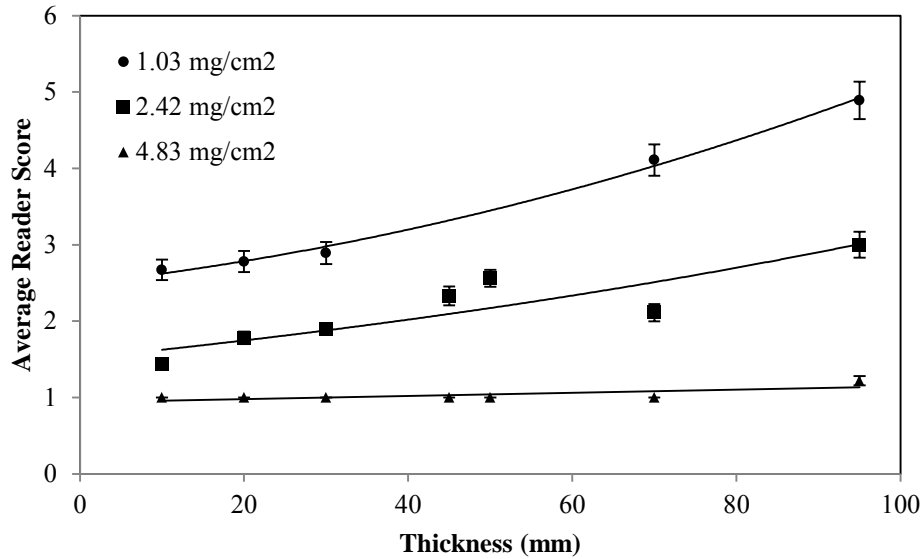


**Figure 6.** Effect of phantom thickness and concentration of lesion on average reader score of detectability. Obvious outliers were excluded from the figure

### 3.2 Effect of focal plane

The metric  $D$  for each lesion was defined as the difference in SDNR between the in-focus and out-of-focus plane.

$$D = \begin{cases} SDNR_{F2} - SDNR_{F1} & , \text{ for lesions in G2} \\ SDNR_{F1} - SDNR_{F2} & , \text{ for lesions in G1} \end{cases}$$

There was found to be little dependence of  $D$  on the lesion size, areal concentration or volumetric concentration.

Next, the reader scores for individual lesions were analyzed to determine if the lesion was better observed in the in-focus plane. A paired student t-test was performed on the reader scores for the two focal planes. This calculation was repeated for each lesion concentration, and the  $p$ -value is shown in Table 2. The differences in detectability between the two focal planes can be considered significant ( $p < 0.05$ ) except for three areal concentrations: 1.6, 4.03 and 4.83  $\text{mg}/\text{cm}^2$ . In retrospect, these correspond the two largest lesions that span almost the entire depth of the iodine insert. In this case, either focal plane will pass through the lesion resulting in similar reader performance.

**Table 2.** Probability associated with a student's paired t-test for the various iodine lesions. Lesions whose  $p$ -value was considered to be significant ( $p < 0.05$ ) are bolded.

Areal Concentration ( $\text{mg}/\text{cm}^2$ )	1.03	1.24	1.6	2.01	2.06	2.42	2.47	3.12	4.03	4.83
<b>p</b>	0.031	0.023	0.78	0.022	0.022	0.009	0.011	0.0063	0.17	0.70

### 3.3 Relationship between SDNR and Reader Score

For each iodine concentration, the average reader score and SDNR are plotted in Figure 7 and fit to a second-order polynomial. The observer scores were found to correlate well with the calculated SDNR values for each of the iodinated lesions. Lesions whose SDNR was higher than 3 were considered to be perfectly visible in terms of area and boundary. Lesions with SDNR below 1 were difficult to distinguish from the background and were in general not visible. Lesions with intermediate SDNR values were visualized but not confidently delineated from the surrounding background.

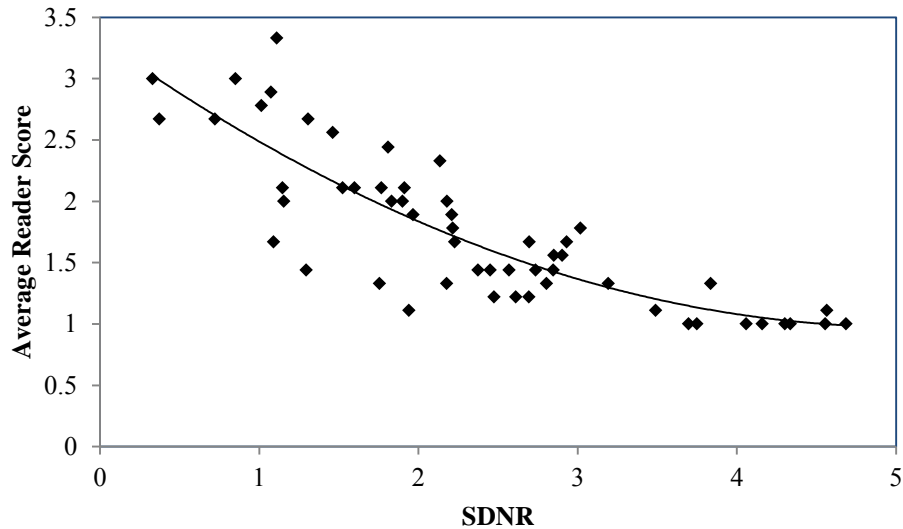


Figure 7. Relationship between SDNR and average reader score for all the concentrations of iodine

#### 4. DISCUSSION AND CONCLUSIONS

The purpose of the study was to identify the relationship between SDNR and detectability of iodinated lesions in CE-DBT. To that end, a physical phantom with a section containing known concentrations of iodinated lesions was imaged on a clinically-available CE-DBT system. Dual-energy images were obtained with and without the iodine insert to simulate pre- and post-contrast image sets. These images were then subtracted to create a HDE tomographic stack to remove the effects of scatter and other misregistration artifacts.

The SDNR and average reader detectability of the lesions was found to increase with increasing concentrations of iodine. The two relationships are illustrated in Figures 4 and 6. If the SDNR values are fitted to a line, the equation can be used as a calibration to quantify the concentration of iodine in the HDE images. The slope of the linear fit,  $S$ , was found to decrease linearly with increasing thickness of the breast phantom (as seen in Figure 5). This relationship can be attributed to secondary effects such as beam hardening and x-ray scatter, both of which are more influential at larger thicknesses. Similar relationships between SDNR, areal concentration of iodine, and thickness were observed by Arvanitis *et al* [13] and Xu *et al.* [14] for contrast-enhanced mammography.

The higher lesion concentrations were easily visible at all thicknesses, while the lower concentrations were progressively harder to distinguish as the thickness of the phantom increased. This effect is most evident at the lowest concentration studied ( $1.03 \text{ mg/cm}^2$  – black circles in Figure 6). This trend is closely correlated to that of SDNR. The detectability of lesions in CE-DBT, whether by an ideal (SDNR) or real observer (Average Reader Score) increases with increasing concentration of iodine and decreasing total thickness of tissue that the lesion is embedded in.

The data from this study suggests that the choice of focal plane does not have a statistically significant impact on the SDNR. The metric  $D$  was calculated as the difference in SDNR between the in-focus and out-of-focus plane for each lesion.  $D$  was not found to be significantly different from 0 for the majority of the lesions, and shows little dependence on lesion size, areal or volumetric concentration.

The observer study was, however, able to describe a relationship between the choice of focal plane and the average readers score. As demonstrated in Table 2, the average detectability score was found to vary with statistical significance ( $p < 0.05$ ) from F1 to F2 for 7 out of 10 lesions. This implies that these seven lesions were better observed in the in-focus plane, as anticipated. The other 3 lesions had average scores for F1 and F2 that could not be deemed to be statistically different from each other. Out of the three lesions in question, two were from lesions with the two highest areal concentrations of iodine ( $4.03$  and  $4.83 \text{ mg/cm}^2$ ). These lesions possess enough x-ray contrast that they are easily

detectable even if the tomographic slice chosen does not correspond to their physical location in the phantom. Thus, the plane of focus has been found to have a profound effect on the reader score. These lesions were also two of the largest in physical diameter and spanned almost the entire depth of the iodine section of the phantom. Both focal planes will pass through a portion of the lesion, and so the reader score is expected to be similar. Unlike *SDNR*, the observer detectability of lesions was found to be strongly influenced by the choice of focal plane. This can be explained by the fact that the observers were asked to incorporate metrics such as delineation of the boundary and observable area (see Table 1) into their score. Metrics such as just-noticeable difference (JND) may be better suited to predict lesion detectability.

The correlation between *SDNR* and average reader score is shown in Figure 7. As the *SDNR* increases, the visibility of the lesions increases. The data points can be stratified into three groups: (i) *SDNR* is less than 1, (ii) *SDNR* is between 1 and 3, (iii) *SDNR* is greater than or equal to 3. An *SDNR* of 1 corresponds to a per-pixel signal difference that is equivalent to the standard deviation of the background signal. From the data, lesions with an *SDNR* less than 1 were recorded with a score that corresponds to partial recognition of the area and boundary and uncertainty of the size. This indicates that lesions whose signal compared to the background is less than the standard deviation of the background were difficult to distinguish. Lesions with *SDNR* greater than 3 were perfectly visible in terms of size, area, and boundary. Lesions with intermediate values of *SDNR* were visualized but not confidently separated from the surrounding background. Thus, a lesion must consist of an average signal that is at least three standard deviations away from the background in order for a reader to confidently detect the object.

This study is able to clearly demonstrate that the same factors which influence *SDNR* of iodinated lesions in CE-DBT also affect reader detectability. Studies that aim to optimize the imaging parameters in CE-DBT can use the computed threshold value of *SDNR* to quantify the minimum detectable concentration of iodine using their approach.

## 5. REFERENCES

1. Nunes LW, Schnall MD, Siegelman ES, Langlotz CP, Orel SG, Sullivan D, *et al.* Diagnostic Performance Characteristics of Architectural Features Revealed by High-Spatial Resolution MR Imaging of the Breast. *American Journal of Roentgenology*. 1997 Aug; 169:409-415
2. Kuhl CK, Nielcareck P, Klaschnik S, Leytner C, Warelmann E, Gieseke J, *et al.* Dynamic Breast MR Imaging: Are Signal Intensity Time Course Data Useful for Differential Diagnosis of Enhancing Lesions. *Radiology*. 1999 Oct; 211:101-110
3. Schnall MD, Blume J, Bluemke DA, DEAngelis GA, DeBruhl N, Harms S, *et al.* Diagnostic Architectural and Dynamic Features at Breast MR Imaging: Multicenter Study. *Radiology*. 2006 Jan; 238:42-53
4. Carton AK, Ullberg C, Lindman K, Acciavatti R, Francke T, Maidment ADA. Optimization of a dual-energy contrast-enhanced technique for a photon-counting digital breast tomosynthesis system: 1. A theoretical model. *Med Phys*. 2010 Nov; 37(11): 5896 -5907
5. Carton AK, Ullberg C, Maidment ADA. Optimization of a dual-energy contrast-enhanced technique for a photon-counting digital breast tomosynthesis system: II. An experimental validation. *Med Phys*. 2010 Nov; 37(11):5908-5913
6. Carton AK, Gavenonis S, Currivan JA, Conant E, Schnall MD, Maidment ADA. Dual-energy contrast-enhanced digital breast tomosynthesis – a feasibility study. *British Journal of Radiology*. 2010; 83:344-350
7. Chen SC, Carton AK, Albert M, Conant E, Schnall MD, Maidment ADA. Initial clinical experience with contrast-enhanced digital breast tomosynthesis. *Acad Radiol*. 2007 Feb; 14(2):229-238
8. Samei E, Saunders Jr RS. Dual-energy contrast-enhanced breast tomosynthesis: optimization of beam quality for dose and image quality. *Physics in Medicine and Biology*. 2011; 56:6359-6378
9. Hum Y, Zhao W. A 3D linear system model for the optimization of dual-energy contrast enhanced digital breast tomosynthesis. *Proc of SPIE*. 2011; 7961
10. Kiarashi N, Ghate SV, Lo JY, Nolte LW, Samei E. Application of a Dynamic 4D Anthropomorphic Breast Phantom in Contrast-Based Imaging System Optimization Dual-Energy or Temporal Subtraction. *LNCS*. 2012; 7361:658-665
11. Carton AK, Ullberg C, Derand H, Maidment ADA. Development of a physical 3D anthropomorphic breast phantom. *Med Phys* 2011 Feb; 38(2): 891-896
12. Mankansson M, Svensson S, Zachrisson S. VewDex 2.0: a Java-based DICOM-compatible software for observer performance studies. *Proc of SPIE* 2009; 7263

13. Arvanitis CD, Speller R. Quantitative contrast-enhanced mammography for contrast medium kinetic studies. *Phys Med Biol.* 2009; 54: 6041-6064
14. Xu T, Ducote JL, Wong JT, Malloi S. Feasibility of a real time dual-energy imaging based on a flat panel detector for coronary artery calcium quantification. *Med Phys.* 2006 June; 33(6): 1612-1622